

A 4D Hybrid Algorithm to Scale Parallel Training to Thousands of GPUs

Siddharth Singh, Prajwal Singhania, Aditya K. Ranjan, Zack Sating, Abhinav Bhatele

Department of Computer Science
University of Maryland

E-mail: {ssingh37, prajwal, aranjn2, zsating}@umd.edu, bhatele@cs.umd.edu

Abstract—Large communication costs are a critical bottleneck in training state-of-the-art neural networks on distributed systems. This paper introduces AxoNN, a novel four-dimensional (4D) parallelization approach, inspired by Agarwal’s algorithm for matrix multiplication, for parallelizing tensor computations in deep learning. AxoNN employs two key strategies to minimize communication overhead. First, we optimize communication by overlapping expensive collective operations (reduce-scatter, all-gather, all-reduce) with computations. Our experiments with a 20-billion parameter transformer model demonstrate that these optimizations deliver nearly 53% improvement. Second, we present an analytical model to assist users in identifying communication-minimizing configurations within the vast search space defined by our 4D algorithm. This model empowers practitioners by simplifying the tuning process for their specific training workloads. When training an 80-billion parameter model on 1024 GPUs of Perlmutter, AxoNN surpasses Megatron-LM, a state-of-the-art framework, by a significant 26%. Additionally, it achieves 57% of the theoretical peak FLOP/s.

Index Terms—Parallel deep learning, Tensor parallelism, Communication modelling, Asynchronous communication

I. INTRODUCTION

The effectiveness of deep neural networks in generalization improves reliably with increased size in terms of parameters [1], [2]. This trend has led to the emergence of state-of-the-art AI algorithms relying on neural networks with hundreds of billions of parameters as their foundation [3], [4]. Given the substantial memory requirements for training these models, often exceeding that of a single GPU, the use of GPU-based clusters has become standard. Consequently, it is imperative to develop efficient parallel algorithms and frameworks that can leverage the combined memory capacity and computational power of multiple GPUs for the practical and timely training of such neural networks.

The foremost challenge in scaling parallel or distributed training on multi-GPU supercomputers lies in the substantial communication costs. While modern GPUs have significantly improved computing efficiency, driven by specialized cores such as Tensor Cores in Nvidia GPUs, network bandwidths across nodes have lagged behind. This limitation results in modern frameworks for parallel deep learning inefficient at large scales due to the considerable overheads of message passing. These overheads stem primarily from two factors: the inherent large communication volumes associated with the underlying distributed DL algorithms and inefficient imple-

mentations of message-passing with minimal to no overlap with computation. These challenges pertaining to communication thus impede the efficiency of parallel frameworks at the scale of thousands of GPUs. This scalability is increasingly desirable, particularly considering the compute-intensive nature of modern training workloads such as large language models (LLMs).

In light of the above challenges, we propose AxoNN, a four dimensional (4D) hybrid parallel framework which strives to alleviate the aforementioned performance bottlenecks of existing parallel deep learning frameworks. AxoNN leverages a variation of Agarwal’s well-established parallel matrix multiplication algorithm [5] from high-performance computing (HPC) to efficiently parallelize the compute-intensive matrix multiplications within deep neural networks. While utilizing an efficient parallel matrix multiplication algorithm is a crucial step, it’s not the sole factor in achieving communication efficiency. To tackle this challenge, AxoNN employs a two-pronged approach:

Overlapping Communication and Computation: Many tensor parallelization algorithms, including ours, rely on collective communication operations (reduce-scatter, all-gather, and all-reduces) that can be expensive at scale. To address this, we propose a suite of communication optimizations that leverage asynchronous communication. This allows for significant overlap between communication and computation, maximizing hardware utilization.

Communication-Aware Configuration Selection: The way we decompose work and distribute GPUs across the four dimensions of our algorithm significantly impacts communication costs. To guide users, we introduce a communication model that identifies a small set of communication-optimal configurations. This eliminates the need to explore the entire search space. Users can then efficiently profile these suggested configurations, streamlining the process of finding the optimal settings for their specific workload.

We demonstrate the effectiveness of our framework by performing scaling studies on multi-billion parameter neural networks, and comparing our performance with two state-of-the-art tensor parallel frameworks - Megatron-LM [6] and DeepSpeed [7], [8] across Nvidia and AMD GPUs. In a weak scaling study on GPTs with parameters in the range from 5B–80B on 64-1024 GPUs, we observe significant performance

improvements of 25–45% over Megatron-LM and 32–50% over DeepSpeed on Nvidia GPUs, and 23–35% over DeepSpeed on AMD GPUs. We demonstrate that our method scales well, even on AMD GPUs, where other frameworks struggle. We also show significant improvements when training UNet CNNs in a weak scaling study when compared to ZeRO-3 [8].

In summary, our contributions can be summarized as follows:

- A scalable four-dimensional (4D) hybrid parallel framework, AxoNN, which exhibits less communication volume compared to its counterparts.
- A communication model tailored to assist users in discovering communication-minimizing configurations for the 5D algorithm.
- An optimized implementation of the communication in our proposed algorithm, that maximizes overlap between computation and communication by leveraging asynchrony and intelligent communication scheduling.

II. BACKGROUND AND RELATED WORK

This section provides a background on different frameworks and algorithms for parallel deep learning training, primarily focusing on tensor parallelism and communication pattern modelling.

A. Tensor Parallelism

Tensor parallel algorithms work by parallelizing the computation of every layer of the neural network. Most frameworks for tensor parallelism focus on fully-connected (FC) and/or convolution layers. This is because most of the other layer types in neural networks like activation [9], [10] or norm functions [11]–[13] are embarrassingly parallel and thus trivial to parallelize. The most widely used tensor parallel framework is Shoeybi et al.’s Megatron-LM [6]. In their work the authors propose an algorithm to parallelize a pair of FC layers. They apply their technique to parallelize large GPT style transformers efficiently within GPUs in a node. Their framework has been widely used to train some of the largest language models in existence like Megatron-Turing-NLG-530B [4], Bloom-175B [14], and Turing-NLG [8]. However, their approach becomes inefficient for models that do not fit on a single node [15]. As a result, a number of other works have proposed recently that attempt to alleviate this issue. Qifan et al. propose a 2D tensor parallel algorithm for FC layers [16] based on the SUMMA algorithm for distributed matrix multiplication. Similarly, Wang et al. propose a 2.5D parallel algorithm for FC layers [17]. Zhengda et al. introduce a 3D tensor parallel algorithm based on Agarwal’s distributed matrix multiplication [5]. Jangda et al. develop high performance GPU kernels that overlap computation with communication in Megatron-LM’s algorithm [18]. Dryden et al. propose channel and filter parallelism for convolution layers [19]. Wang et al. propose using asynchronous sends instead of all-gather operations for a 2D tensor parallel scheme to overlap communication and computation [20]. Merak [21] introduces an automated 3D

parallel framework based on graph partitioning, along with techniques to overlap communication with computation in pipeline and tensor parallelism modes. Li et. al. propose Oases that overlaps backward pass communication with activation recomputation [22].

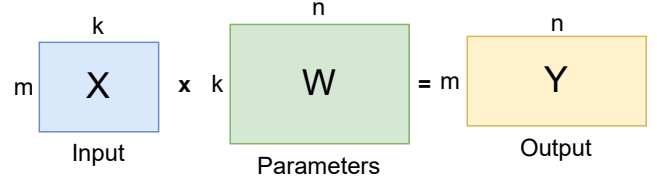


Fig. 1: Computation in the forward pass of a fully-connected (FC) layer with input X and layer parameters W . The output, Y is a matrix multiplication of X and W . We assume $X \in \mathbb{R}^{m \times k}$, $W \in \mathbb{R}^{k \times n}$, and $Y \in \mathbb{R}^{m \times n}$.

B. Communication Modelling

In order to alleviate the complexity of choosing the correct mapping of GPUs to the different parallelism dimensions, several works have proposed automated frameworks that try to model the behavior of the configurations with respect to the communication and computation costs. Alpa [23] is a compiler that automates the process of parallelizing neural networks by coming up with communication efficient strategies for decomposing a given set of GPUs into various forms of parallelism. It models the training task as a computational graph, along with a device mesh and formulate an ILP optimization to minimize the execution cost of each node of the graph. Cheng et al. develop a hierarchical communication matrix over a 2-dimensional device mesh to model the communication cost [24], taking the underlying network topology into account, and use it to automate the decomposition over a 2D tensor parallelism scheme. Li et al. extend Alpa and model the cost of overlapped communication-computation for improving the automated parallel plan [22]. Alok et al. propose parallel algorithms and model communication costs for training Graph Neural Networks [25]. Our communication model aims to provide a simple heuristic for communication time that can be used to guide the choice of parallel configurations similar to [24]. Unlike their model, we try to account for a 3D tensor parallel paradigm, along with data parallelism. To the best of our knowledge, ours is the first work that models communication costs for 3D tensor + data parallelism.

III. DESIGNING A HYBRID TENSOR AND DATA PARALLEL FRAMEWORK

In this section, we provide an overview of AxoNN, our framework for parallelizing the training of neural networks at scale on GPU based supercomputers. AxoNN combines tensor and data parallelism to enable the training of large multi-billion parameter models, such as GPT-3 [3], on hundreds of GPUs, which cannot be trained on a single GPU due to their

significant memory requirements. Our algorithm features a hierarchical design with two levels: data and tensor parallelism. We now provide a detailed description of each level, starting with data parallelism.

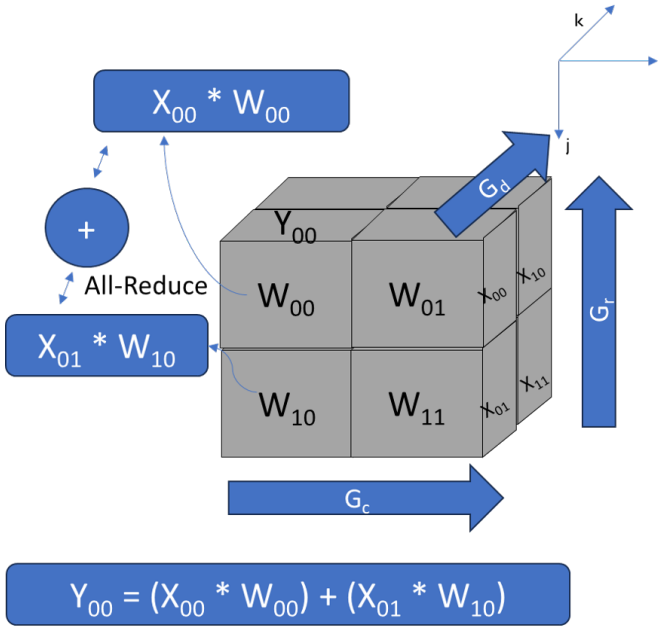


Fig. 2: Parallelization of an FC layer with Agarwal’s 3D parallel matrix multiplication algorithm [5] on eight GPUs organized in a $2 \times 2 \times 2$ topology. We use G_r , G_d , and G_c to refer to the number of GPUs along the three dimensions of the topology, where r,c, and d stand for row, column, and depth respectively.

A. Data Parallelism

A pure data parallel setup (i.e. without other modes of parallelism) involves (1) assigning a full copy of a neural network to every GPU (2) dividing the input batch equally between these GPUs. However, in a hybrid parallel framework like AxoNN, we first organize the total number of GPUs we want to use for training (say G) into groups of equal size. Then, we treat these groups in a similar fashion as single GPUs in pure data parallelism. Specifically, we first assign a unique partition of the input batch to every group. Then, we task these groups to collectively compute the entire neural network on their assigned partitions of the batch. We parallelize this computation within each GPU group by employing tensor parallelism, which forms the second level of our algorithm’s hierarchy. After the computation is completed, the GPU groups synchronize their weights by issuing an all-reduce. Throughout this paper, we use G_{data} to refer to the number of these GPU groups. We use the subscript “data” here, as the degree of data parallelism i.e. the number of parallel partitions of the input batch equals the number of GPU groups. Also, since each GPU group realizes tensor parallelism, we use G_{tensor} to refer to the number of GPUs in each group. Note that G ,

G_{data} , and G_{tensor} satisfy $G = G_{\text{data}} \times G_{\text{tensor}}$. Next, we discuss how AxoNN realizes tensor parallelism in every GPU group with G_{tensor} GPUs.

B. Tensor Parallelism

Now, we discuss how the aforementioned GPU groups compute the entire neural network on their assigned batch shards via tensor parallelism, the second level of our algorithm’s hierarchy. As discussed in Section II, tensor parallel algorithms parallelize the computation of every layer of the neural network across GPUs. Let us now understand how AxoNN’s tensor parallelism computes a single layer in parallel using a fully-connected (FC) layer as an example.

Before we discuss the parallelization of an FC layer, let us look at the serial computation in an FC layer. In Figure 1, we illustrate the computation in the forward pass of an FC layer. We use X and W to represent the layer’s input and parameter matrix, respectively. The forward pass of a FC layer produces Y , which equals the output of the matrix multiplication XW . We assume that the dimensions of X , W , and Y are $m \times k$, $n \times k$, and $m \times n$, where m , k , and n are integers. Similarly, the backward pass involves two matrix multiplication operations $\frac{\partial L}{\partial X} = \frac{\partial L}{\partial Y} \times W^T$ and $\frac{\partial L}{\partial W} = X^T \times \frac{\partial L}{\partial Y}$, where L is the training loss. Thus parallelizing an FC layer entails parallelizing these three matrix multiplication operations across multiple GPUs. Now, let us look at how AxoNN’s tensor parallelism achieves this parallelization.

In this work we use a modified version of Agarwal’s 3D parallel matrix multiplication algorithm [5] for parallelizing the matrix multiplications within FC layers. Now, we know from Section III-A that AxoNN realizes tensor parallelism within groups of GPUs of size G_{tensor} . To realize Agarwal’s algorithm, we first organize the GPUs in these groups in a virtual three dimensional (3D) grid topology of dimensions $G_c \times G_r \times G_d$, where c,r,d stand for column, row and depth respectively. Once again, $G_c \times G_r \times G_d = G_{\text{tensor}}$. As an example, we show a topology of eight GPUs with $G_c = 2$, $G_r = 2$ and $G_d = 2$ in Figure 2. Additionally, we use GPU_{ijk} to refer to a GPU in the grid, where $0 \leq i \leq G_c - 1$, and $0 \leq j \leq G_r - 1$, and $0 \leq k \leq G_d - 1$.

Now let us discuss how Agarwal’s algorithm maps inputs X and parameters W onto this 3D GPU topology. Both X and W are decomposed in a 2D fashion along two of the three dimensions of the algorithm and these partitions are replicated across the third dimension. For example in Figure 2, we observe that the rows and columns of W are partitioned along the r and c axes respectively, whereas the 2D partitions are duplicated across the d axis. Similar for X , we partition the rows and columns across the d and r axes respectively and replicate the 2D partitions across the c axis. In our modified version of Agarwal’s algorithm we propose to shard the W matrix further along the d axis instead of replicating it. This is done to save memory as the set of GPUs along the d axis would only have to store the gradients and optimizer states of unique shards of the parameters. Function `DIVIDE_WEIGHTS` of Algorithm 1 demonstrates

this modified distribution of weights proposed by us. It is important to note that `DIVIDE_WEIGHTS` is called only once at the beginning of training after which the optimizer can operate on the local weight partitions and their gradients for the rest of the training.

Having discussed the distribution of inputs and parameters, let us now discuss the forward and the backward passes using our tensor parallel algorithm. We illustrate the forward pass in function `TENSOR_PARALLEL_FORWARD_PASS` of Algorithm 1, the arguments to which are the input activations X and the local weights of the GPU W'_{ji} . In lines 8-9 we divide the input X as per the semantics of Agarwal’s algorithm. Now since, we had done an extra sharding on W along the d axis, we first reverse it by issuing an all-gather along the depth axis (line 10). Now every GPU computes a matrix multiply of their local partitions of X and W , which is essentially $X_{kj} \times W_{ji}$ for GPU $_{i,j,k}$ (line 11 of Algorithm 1). However, since the columns of X are distributed across the GPUs across the c axis, this step requires a further all-reduce operation between the column GPUs to compute the complete output (line 12 of Algorithm 1). Finally, at the end of the forward pass every GPU caches its local partitions of X and W , as these are required later in the backward pass.

Having discussed the forward pass, let us now focus on the backward pass. $\frac{\partial L}{\partial Y_{ki}}$ is the partial derivative of the loss with respect to the output of the forward pass, which serves as the input to the backward pass. First, we retrieve the local partitions of the data, that we had cached earlier in the forward pass (line 18). After this step, we have all the data in place to begin computing the two matrix multiplications in the backward pass. We start with computing the gradients of the loss with respect to X i.e. $\frac{\partial L}{\partial X} = \frac{\partial L}{\partial Y} \times W^T$. For this, every GPU does a matrix multiplication of their local partition of $\frac{\partial L}{\partial Y}$ and a transpose of their local partition of W (line 19). Just like the forward pass this results in a partial output which needs to be aggregated via an all-reduce. However, in this case the all-reduce is done by GPUs in along the r axis (line 19). Finally, we compute the derivative with respect to the parameters by multiplying the transpose of the local partition of X with the local partition of $\frac{\partial L}{\partial Y}$, and then do a reduce scatter on the outputs so that each GPU ends up with the gradients of their local partitions of the weights (line 20).

Algorithm 1 can be easily extended to convolution layers also by treating k and n the number of input and output channels, respectively. This completes a high level overview of our proposed hybrid parallel algorithm. As discussed in Section I, high communication costs are the primary bottleneck in large scale parallel training of neural networks. In the next two sections of the paper, we discuss two orthogonal strategies to alleviate this bottleneck.

IV. IMPROVING THE PERFORMANCE OF AXONN

In this section, we present communication optimizations aimed at enhancing the performance of the framework discussed in Section III. These optimizations target the reduction

Algorithm 1 Our 3D tensor parallelism for GPU $_{ijk}$ in a $G_c \times G_r \times G_d$ grid. We highlight all communication operations in blue.

```

1: function DIVIDE_WEIGHTS(W)
2:   // Let  $W = \begin{bmatrix} W_{0,0} & W_{0,1} & \cdots & W_{0,G_c-1} \\ \vdots & \vdots & \vdots & \vdots \\ W_{G_r-1,0} & W_{G_r-1,1} & \cdots & W_{G_r-1,G_c-1} \end{bmatrix}$ 
3:    $W'_{ji} = \text{Get } W_{ji}$  and shard it further along the depth tensor
   parallel group
4:   return  $W'_{ji}$ 
5: end function
6:
7: function TENSOR_PARALLEL_FORWARD_PASS( $X, W'_{ji}$ )
8:   // Let  $X = \begin{bmatrix} X_{0,0} & X_{0,1} & \cdots & X_{0,G_c-1} \\ \vdots & \vdots & \vdots & \vdots \\ X_{G_d-1,0} & X_{G_d-1,1} & \cdots & X_{G_d-1,G_c-1} \end{bmatrix}$ 
9:   Get  $X_{kj}$ , if not in memory
10:   $W_{ji} = \text{All-Gather}_{\text{depth}}(W'_{ji})$ 
11:   $Y'_{ki} = X_{kj} \times W_{ji}$ 
12:   $Y_{ki} \leftarrow \text{All-Reduce}_{\text{column}}(Y'_{ki})$ 
13:  // Cache  $X_{kj}$  and  $W_{ji}$  for the backward pass
14:  return  $Y_{ki}$ 
15: end function
16:
17: function TENSOR_PARALLEL_BACKWARD_PASS( $\frac{\partial L}{\partial Y_{ki}}$ )
18:  Retrieve  $X_{kj}$  and  $W_{ji}$  from cache
19:   $\frac{\partial L}{\partial X_{kj}} \leftarrow \text{All-Reduce}_{\text{row}}(\frac{\partial L}{\partial Y_{ki}} \times W_{ji}^T)$ 
20:   $\frac{\partial L}{\partial W_{ji}} \leftarrow \text{Reduce-Scatter}_{\text{depth}}(X_{kj}^T \times \frac{\partial L}{\partial Y_{ki}})$ 
21:  return  $\frac{\partial L}{\partial X_{ij}}, \frac{\partial L}{\partial W_{jk}}$ 
22: end function

```

of communication time for a given training workload, consisting of the neural network, its hyper parameters, and the number of GPUs, along with a predefined configuration of our proposed 4D algorithm. Later in section V, we discuss how to configure the four dimensions of our algorithm for a given training workload. However, for now, we assume that these dimensions are predetermined. As a running example, we consider a 20B parameter GPT style transformer [3] with a batch size of 32k tokens (sequence length of 2k tokens) on 16 GPUs or four nodes of the Perlmutter supercomputer. We use a configuration of $G_c = 2$, $G_r = 2$, $G_d = 4$, and $G_{data} = 1$

A. Optimization A: Eliminating Communication at Layer Boundaries

Our first optimization aims to eliminate unnecessary communication at layer boundaries. Let us first understand why said communication happens in the first place. As shown in Figure 2, the inputs X and outputs Y of a tensor parallel FC layer are sharded in different ways across the 3D tensor parallel topology. Now, if we have another FC layer that takes as input the output of the FC layer in Figure 2, we would have

Breakdown of Batch Times for GPT-20B on 16 GPUs of Perlmutter

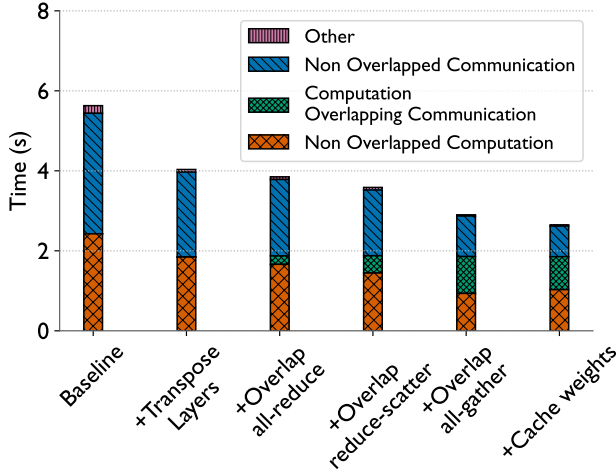


Fig. 3: Studying the effect of the proposed communication optimizations on the training batch times of a GPT 20B model on 16 GPUs of Perlmutter. We use a batch size of 32k tokens with a sequence length of 2048. We use Pipit [26] for generating these distributions from trace data.

to redistribute Y such that it is sharded in the same way as X . This is exactly why we would need extra communication at layer boundaries. To eliminate this, we propose a simple solution - for every alternate FC (or convolution) layer in the neural network, we transpose the weight matrix W such that its columns are distributed across the row tensor parallel axis and rows are distributed across the column tensor parallel axis. This makes it such that the outputs of a layer are automatically in the correct position to serve as inputs to its successor layer. Note that we only have to do the weight transposes once at the beginning of the training. In Figure 3, we study the effect of this optimization on our running example, with the baseline representing the case where we do extra communication to redistribute the outputs, and the Optimization A representing the case where we transpose the weights of every alternate layer. We observe a significant improvement of 28.39% in the batch times.

B. Optimization B: Row and Column Parallel All-Reduces

Optimization B is concerned with overlapping the all-reduce communication in the backward pass of a layer across the row tensor parallel group (Line 19 of Algorithm 1) with computation. Note that for transposed layers discussed in the previous section, this communication would happen across the column tensor parallel groups. Our strategy to achieve overlap is to issue the all reduce in line 19 asynchronously and overlap it with the computation of the weight gradients happening in line 20. Once this computation has finished, we wait on the asynchronous all reduce to finish. From figure 3, we can see that adding this optimization improves batch times by a further 4.73%.

C. Optimization C: Depth Parallel Reduce-Scatters

Next we look at optimizing the reduce scatters in the backward pass (Line 20 of algorithm 1). The outputs of this reduce scatter are the gradients of the loss w.r.t. the weights of the layer. Note that these aren't required until we have finished the backward pass of the entire network and are ready to do the all-reduces pertaining to data parallelism. Taking advantage of this we 1. issue these reduce scatters asynchronously and 2. only wait on them to complete once all layers have finished their backward pass. This allows us to overlap the reduce scatter of one layer with the backward pass compute of its predecessors. From figure 3, we can see that adding this optimization improves batch times by a further 7.78%.

D. Optimization D: Depth Parallel All-Gathers

Our next optimization aims to overlap the all-gather operations in the forward pass (Line 10 of Algorithm 1) with computation. It's important to note that this all-gather operation doesn't depend on intermediate outputs of the forward pass. Leveraging this independent nature of the all-gather, we propose pre-emptively enqueueing the all-gather operation for the next layer while the computation for the current layer is ongoing. At the outset of training, we generate a topological sort of the neural network computation graph to determine the sequence for performing the all-gathers. Subsequently, we execute them preemptively as outlined earlier. In figure 3, we observe that overlapping the all-gathers in this fashion leads to a significant improvement of 18.82%!

E. Optimization E: Caching Outputs of All-Gathers

Our next optimization exploits the fact that most large scale training runs involve using activation checkpointing [], which basically is a method to significantly reduce activation memory usage albeit at an effective cost of an extra forward pass through the network. Since the parameters across the two forward passes are not changing, we can see that the all-gathers in line 10 produces the same output in the two forward passes. To eliminate the second all-gather we propose to cache the outputs of the first all-gather and reusing them during the second forward pass. For our running example of the 20B model, we cache the all-gather outputs of 28 out of the 32 transformer encoder layers and observe an improvement of 8.99%. Overall, the five proposed optimizations in this section improve the batch times by a significant 53% over the baseline!

V. PERFORMANCE MODEL OF COMMUNICATION

In the previous section, we discussed various strategies to minimize the time spent in communication, given a training workload and fixed values of the four dimensions of our algorithm. Now, we address an orthogonal but equally important question - *how can we configure the four dimensions of our 4D algorithm to minimize total communication time for a given training workload?*. To tackle this challenge, we introduce a communication model that quantifies the total communication time as a function of the training workload, the

four configuration parameters, and the bandwidths within the multi-GPU cluster. Subsequently, to identify a small set of (say five) near-optimal configurations, one can apply our analytical communication model across the entire range of possible configurations and select the top five with the lowest predicted communication times. This approach offers significant time savings compared to exhaustively running all configurations within the 4D search space in a brute force manner. Now, let us begin by first outlining the assumptions of our communication model.

- *Assumption-1:* All-reduce, reduce-scatter, and all-gather collectives are implemented using the bandwidth-optimal ring algorithm [27].
- *Assumption-2:* For inter-node collectives, the underlying communication library minimizes the number of links of the ring crossing node boundaries.
- *Assumption-3:* We assume that the messages are large enough such that the latencies can be ignored. In other words, if process 1 is sending a message of n bytes to process 2, then we assumed that the transmission time is simply $\frac{n}{\beta}$, where β is the available bandwidth between the two processes.
- *Assumption-4:* We assume all messages are synchronous, ignoring any overlap of computation and communication
- *Assumption-5:* We assume a constant bidirectional bandwidth β_{inter} between every pair of nodes.
- *Assumption-6:* The total number of GPUs, the number of GPUs per node, as well as the sizes of the four dimensions of our algorithm are all powers of two.

Some of these assumptions may initially seem overly restrictive for accurately estimating communication times. For instance, given the multiple overlap optimizations proposed by us in Section IV, our assumption of all communication being synchronous is obviously inaccurate. However, note that we're not aiming to model precise communication times down to the microsecond. Instead, our goal is more modest: to identify a small set of perhaps five near-optimal configurations of our 4D algorithm for a given training workload. In this context, the communication model we propose, as we'll demonstrate later in this section, serves as a valuable tool for achieving our objectives. Now, let's discuss the specifics of our proposed communication model.

For an all-reduce operation with buff_{sz} as the size of the input buffer on each GPU, p as the number of participating processes, and β_{AR} as the available communication bandwidth, the time it takes to do an all-reduce with the ring algorithm, (say t_{AR}) is:

$$t_{\text{AR}} = \frac{2}{\beta_{\text{AR}}} \times \frac{p-1}{p} \times \text{buff}_{\text{sz}} \quad (1)$$

As mentioned previously, we ignore the latency component of the communication. Similarly, for reduce-scatter, this time (say t_{RS}) is half of t_{AR} :

$$t_{\text{RS}} = \frac{1}{\beta_{\text{RS}}} \times \frac{p-1}{p} \times \text{buff}_{\text{sz}} \quad (2)$$

Finally, for all-gathers t_{AG} can be expressed as:

$$t_{\text{AG}} = \frac{1}{\beta_{\text{AG}}} \times (p-1) \times \text{buff}_{\text{sz}} \quad (3)$$

Now, let us try to model all of the collectives in AxoNN, starting with the all-gather operation (lines 10 of Algorithm 1). Remember from Figure 1, that the dimensions of the input X , the parameters W , and the output Y are $m \times k$, $k \times n$, and $m \times n$ respectively. The input to this all-gather operation is a $\frac{kn}{G_c \times G_r \times G_d}$ sized shard of the weight matrix. The number of participating processes, p is G_d , and let us assume that the available bandwidth is β_d . Then,

$$t_{\text{layer,AG}} = \frac{1}{\beta_d} \times (G_d - 1) \times \frac{kn}{G_c \times G_r \times G_d} \quad (4)$$

Now for the reduce-scatter in line 20 of Algorithm 1, the input is the same size as the output of the previous all-gather operation $\frac{kn}{G_c \times G_r \times G_d}$. The number of participating processes, p is G_d , and we assume the same bandwidth as before available to the depth tensor parallel groups.

$$t_{\text{layer,RS}} = \frac{1}{\beta_d} \times \frac{(G_d - 1)}{G_d} \times \frac{kn}{G_c \times G_r} \quad (5)$$

Finally, there are three all-reduce operations as mentioned previously. For the all-reduce in line 12 of Algorithm 1, this operation takes place within the row tensor parallel groups, on slices of the output Y of size $\frac{m \times n}{G_d \times G_c}$. Thus,

$$t_{\text{layer,AR-1}} = \frac{2}{\beta_r} \times \frac{(G_r - 1)}{G_r} \times \frac{mn}{G_d \times G_c} \quad (6)$$

Now, for the all-reduce in the backward pass of Algorithm 1 (line 19), the message is a slice of the gradients of the input of size $\frac{m \times k}{G_d \times G_r}$, and this communication happens within the column tensor parallel groups. Thus,

$$t_{\text{layer,AR-2}} = \frac{2}{\beta_c} \times \frac{(G_c - 1)}{G_c} \times \frac{mk}{G_d \times G_r} \quad (7)$$

Finally after the backward pass of Algorithm 1 has finished, GPUs in data parallel groups issue an all-reduce on their local weight gradients. Here the input to the all-reduce is the local shard of the weights of size $\frac{kn}{G_c \times G_r \times G_d}$, and the process group size is G_{data} . Thus,

$$t_{\text{layer,AR-3}} = \frac{2}{\beta_{\text{data}}} \times \frac{G_{\text{data}} - 1}{G_{\text{data}}} \times \frac{mk}{G_d \times G_r \times G_c} \quad (8)$$

Now the total communication time for a layer, t_{layer} is simply the sum of Equations 4, 5, 6, 7, and 8:

$$t_{\text{layer}} = t_{\text{layer,AG}} + t_{\text{layer,RS}} + t_{\text{layer,AR-1}} + t_{\text{layer,AR-2}} + t_{\text{layer,AR-3}} \quad (9)$$

For layers 'transposed' as per the optimization discussed in Section IV-A, one simply needs to swap the values of G_r

and G_c . And finally to model the communication time for the entire model we simply apply Equation 9 to all of its layers.

Our model currently lacks a crucial element: modeling the specific bandwidths ($\beta_r, \beta_c, \beta_d, \beta_{data}$) used in Equations 4 through 8 for a given cluster configuration. To model bandwidths for each process group, we assume the hierarchical organization of process groups: column tensor parallelism (innermost), followed by row tensor parallelism, depth tensor parallelism, and data (outermost). This hierarchical organization is a heuristic choice based on communication patterns. Depth-tensor parallel groups can fully overlap communication (see sections IV-C and IV-D) with computation, unlike row and column parallelism where only backward pass all-reduces can overlap (see section IV-B). As depth-tensor parallelism handles expensive inter-node communication more efficiently, we assign it a higher level in the hierarchy. We adhere to the established practice of placing data parallelism in the outermost communication hierarchy.

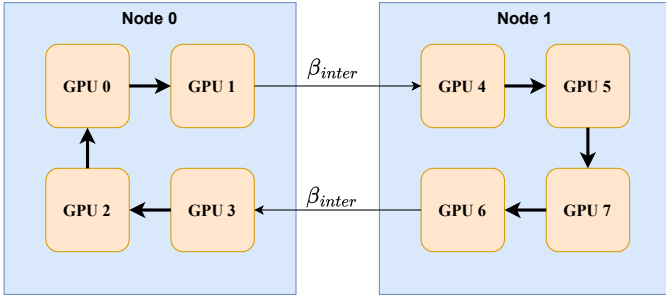


Fig. 4: This figure illustrates a ring-all reduce operation involving eight GPUs, divided across two nodes with four GPUs each. Consistent with Assumption-2, the communication pattern minimizes the number of transmissions crossing node boundaries (shown between GPU 1 and 4, and GPU 6 and 3)

Within our established hierarchical organization for process groups, let’s explore how we model the corresponding bandwidths. We’ll begin with the innermost group, defined as the first level in the hierarchy containing multiple processes (size greater than one). Consider an example with eight GPUs doing an all-reduce with four GPUs on each node (Figure 4). Consistent with Assumption-2, the communication pattern minimizes cross-node links. This optimized layout allows the links crossing node boundaries to fully utilize the available inter-node bandwidth (β_{inter}) for the all-reduce operation (Assumption-5: constant bidirectional bandwidth). Therefore, for the innermost process group, we simply model the bandwidth as β_{inter} , provided its size is greater than the number of GPUs per node. For cases where the entire innermost group fits on a single node, we retrieve bandwidth values from an offline database containing pre-profiled results (with a large message size).

Building on our understanding of the innermost group, let’s explore bandwidth modeling for higher levels in the hierarchy. Consider this scenario: We maintain the eight-GPU setup, but

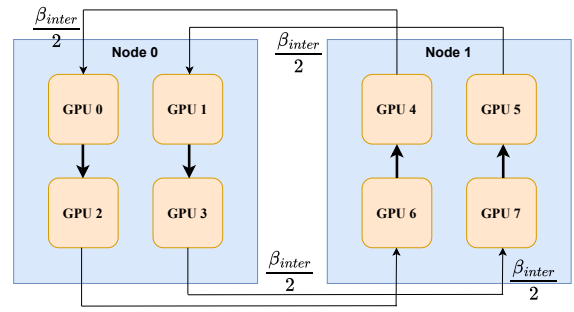


Fig. 5: Two simultaneous ring all-reduces contending for the inter-node bandwidth. This scenario occurs for process groups that are at higher levels in the hierarchy.

the process group of interest is now size four and resides at a higher level in the hierarchy. Additionally, assume the cumulative product of the sizes of all process groups below it in the hierarchy is two. We demonstrate this in Figure 5. At this level of the hierarchy, GPUs 0,2,4,6 form one of the process groups and GPUs 1, 3,5,7 form the other, and we want to model the bandwidths for the collective communication in these groups.

Notice how, unlike the innermost group case, two rings contend for the same inter-node bandwidth (β_{inter}). This competition reduces the effective bandwidth available to each ring link to $\frac{\beta_{inter}}{2}$. If the cumulative product of inner groups were four, the bandwidths would be further reduced to $\frac{\beta_{inter}}{4}$, as we would have had four rings contending for the inter-node bandwidth between these two nodes. Note that cumulative products larger than four wouldn’t degrade bandwidths further as only four ring links can cross between two nodes at a time. This brings us to our general rule for modelling bandwidths for process groups at higher levels in the hierarchy. If the participating processes are situated across nodes, then the modelled bandwidth is $\frac{\beta_{inter}}{\min(cp_{inner}, G_{node})}$, where cp_{inner} is the cumulative product of the sizes of all of the inner process groups, and G_{node} is the number of GPUs on a node. Once again, if the process group wholly resides within a node, we simply retrieve the bandwidth values from an offline database containing pre-profiled results.

Now that we have explored the inner workings of our communication model, let’s evaluate its effectiveness in achieving our key objective: recommending a small, select set (e.g., five) of near-optimal configurations for a given training workload. To study this, we first collect the batch times for all possible parallel configurations of AxoNN, for training two transformer models of size 20 billion and 40 billion parameters on 32 and 64 GPUs of the Perlmutter supercomputer respectively. We classify a configuration as efficient if its batch time falls within 10% of the most optimal configuration’s time or if it ranks among the top-5 configurations sorted by batch times. Finally, to evaluate our communication model’s effectiveness in recommending efficient configurations, we report the average precision@5 for retrieving the so-called efficient

configurations successfully. This metric essentially measures the model’s ability to identify and prioritize these efficient configurations among all possible options. As a baseline for comparison, we also consider the ‘bandwidth-agnostic’ case of our model. Here, we set all bandwidths to one, similar to the approach taken by Zhang et al. [23]. We demonstrate these results in Table I.

TABLE I: Comparison of Average-Precision@5 scores for the Bandwidth-Agnostic and Bandwidth-Aware communication models for various GPT style transformers on Perlmutter. We use a batch size of 65k tokens with a sequence length of 2048.

Neural Network	GPUs	BW-Agnostic Model	BW-Aware Model
GPT-20B	32	0.61	0.96
GPT-40B	64	0.29	1.0

Our bandwidth-aware model achieved significantly higher average-precision@5 scores compared to the bandwidth-agnostic baseline. For the 20 billion and 40 billion parameter models, the bandwidth-aware model achieved scores of 0.96 and 1.0, respectively, compared to just 0.61 and 0.29 for the bandwidth-agnostic model. This substantial improvement suggests that incorporating bandwidth considerations into our model significantly enhances its ability to recommend efficient configurations.

VI. EXPERIMENTAL SETUP

This section provides a detailed account of our empirical evaluation of AxoNN. Our experiments were conducted on two supercomputers, Perlmutter and Frontier. On Perlmutter, each node is equipped with four NVIDIA A100 GPUs, each with a DRAM capacity of 40GB. Additionally, each node on Perlmutter has four HPE Slingshot 11 NICs, with each NIC capable of link speeds of 200 Gb/s. Each A100 GPU is capable of delivering a peak half-precision throughput of 312 TFlop/s. On Frontier, each node has four AMD Instinct MI250X GPUs each with 128GB of high-bandwidth memory. Each node on Frontier also has four HPE Slingshot 11 NICs, with each NIC capable of link speeds of 200 Gb/s. Each MI250X GPU is capable of delivering a peak half-precision throughput of 383 TFlop/s.

A. Description of Neural Networks and Hyper parameters

We evaluate the effectiveness of our proposed framework by conducting experiments on two well-known neural network architectures: U-Net [28] and GPT [3]. U-Nets are fully convolutional neural networks that have diverse applications in various fields such as text-to-image systems (e.g., Dall-E-2 [29] and Stable-Diffusion [30]), image segmentation [31], and object detection [32]. The GPT architecture is a transformer neural network [33] that has been employed in developing several language models [3], [4], [14], [34]. Tables II and III detail the model architectures and their corresponding hyper parameters. For training GPTs, we turn on activation checkpointing due to their large memory requirements [35].

TABLE II: List of U-Net models [28] that we employed in our weak scaling experiments on Perlmutter. Consistent with Nichol et al. [36], our models consist of four levels, with each level comprising three residual blocks. The training batch size to 2048 and the image resolution to 32×32 .

Model	Channels	# GPUs
U-Net 250M	256	64
U-Net 500M	416	128
U-Net 1B	512	256
U-Net 2B	768	512
U-Net 4B	1024	1024

TABLE III: Architectural details of the GPT-style transformers [3] that we use in this work.

Model	#Layers	Hidden-Size	# Heads
GPT 5B	24	4096	32
GPT 10B	32	5120	40
GPT 20B	32	7168	56
GPT 40B	38	9216	72
GPT 80B	42	12288	96

First, to validate AxoNN, we train a small 50M parameter U-Net on the CIFAR-10 dataset [37] for 12000 iterations as well as a 125M parameter GPT-3 on the Bookcorpus dataset for upto 14000 iterations and present the training losses for both of them. We then conduct weak scaling experiments with the U-Net, starting with a 250M parameter model on 64 GPUs, and scaling all the way upto 4B parameters on 1024 GPUs. Note that we had to make slight adjustments to layers and hidden-sizes of GPTs listed in Table III for Megatron-LM because it requires the number of layers to be divisible by the pipeline parallelism dimension. We conduct these U-Net and GPT weak scaling experiments on both Perlmutter and Frontier. Additionally, we also conduct a strong scaling experiment for a 80B GPT-3 going from 64 GPUs to 1024 GPUs on both supercomputers.

When using AxoNN on Perlmutter, we use Megatron-LM [6] as the starter code which we integrate it with. However, we were in correspondence with ML researchers who reported training instability with Megatron-LM on Frontier. So we instead used LitGPT [38] as the starter code there in which we integrated AxoNN as a backend.

B. Choice of Baseline Frameworks

We compare the performance of our proposed hybrid parallel framework with three state-of-the-art baseline frameworks: Megatron-LM [6] and DeepSpeed-3D [39] for tensor parallelism; ZeRO-3 [8] for Fully Sharded Data Parallelism. Megatron-LM proposes tensor parallelism for fully-connected layers and applies their method to train multi-billion parameter GPT-style transformers. Their framework has been used to some of the largest neural networks studied in the literature, including Megatron-Turing-NLG-530B [4], Bloom-175B [14], and Turing-NLG [8]. ZeRO-3 is stage 3 of the ZeRO optimizer which partitions the optimizer states, gradients, and parameters. DeepSpeed-3D combines ZeRO-powered

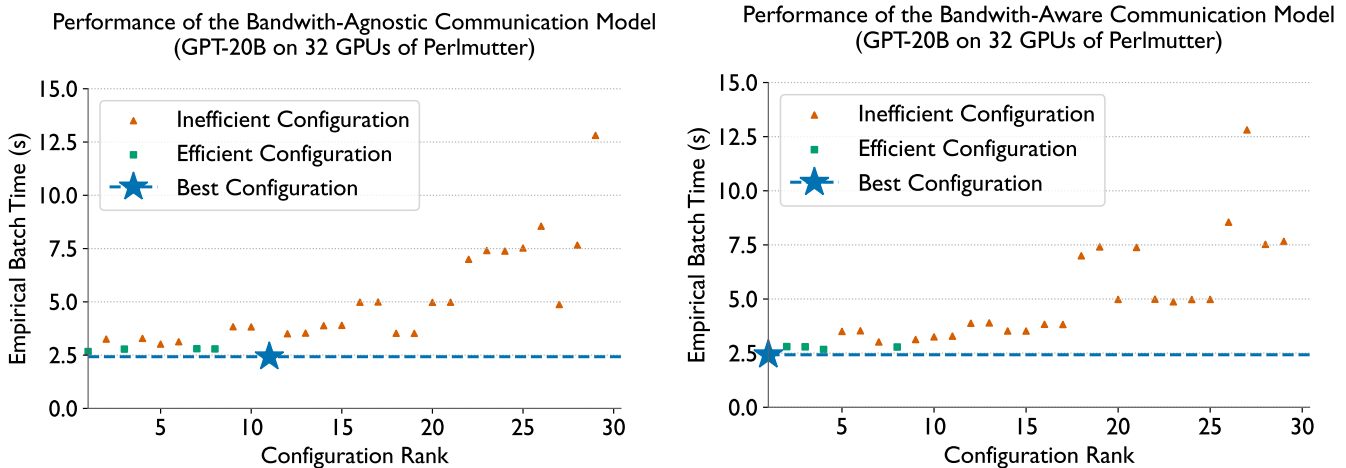


Fig. 6: Comparison of empirical batch times across different configurations, ranked by both bandwidth-agnostic (left) and bandwidth-aware communication models (right). Notably, four out of the top five configurations identified by the bandwidth-aware model are efficient, while the bandwidth-agnostic model only recognizes two. Additionally, the optimal configuration ranks first in the bandwidth-aware model but twelfth in the bandwidth-agnostic model.

data parallelism, pipeline parallelism, and tensor-slicing model parallelism.

C. Evaluation Metrics

For our weak and strong scaling experiments we report the average time per iteration. We do so by running each framework for ten batches and reporting the average of the last five. For our runs, we also calculate the percentage of peak half precision flop/s. To do so, we first re purpose Narayanan et al. 's [15] analytical formulation for the number of floating point operations in a transformer. We then divide it by the average iteration time and the number of GPUs to get the flop/s per GPU. Finally, on Perlmutter, we divide this quantity by 312 Tflop/s, which is the peak half-precision flops for an A100 GPU, to obtain the percentage of peak flop/s. We do similar calculations on Frontier.

VII. RESULTS

In this section, we describe the results of the empirical experiments outlined in Section VI.

TABLE IV: Hardware flop/s utilization for weak scaling of GPTs on Perlmutter. We use a batch size of 4M tokens and a sequence length of 2048.

#GPUs	Model	Megatron-LM	ZeRO-3	DeepSpeed-3D	AxoNN
64	GPT-5B	37%	55%	33%	67%
128	GPT-10B	42%	57%	33%	63%
256	GPT-20B	42%	57%	35%	67%
512	GPT-40B	44%	55%	35%	64%
1024	GPT-80B	42%	27%	38%	57%

A. Validating Our Implementation

We want to ensure that parallelizing a neural network using AxoNN does not affect its statistical efficiency. Therefore, to establish the correctness of our implementation, we present

the loss curves for a 125M parameter GPT-3 and a 50M parameter UNet model trained on 16 GPUs using AxoNN in the left and right sides of Figure 7 respectively. For both the experiments, we set G_c , G_r , G_d , and G_{data} to two, two, two and two, respectively, such that all of the dimensions of our algorithm are active. We also switch on all of the communication optimizations discussed in Section IV.

For the GPT experiment, we compare with Megatron-LM, with the degree of data parallel parallelism set to sixteen. We observe that AxoNN successfully trains the model to convergence and produces near identical loss curves with Megatron-LM, thus validating our implementation. For the UNet experiment, we compare with pure data parallelism of degree eighth. Again, we observe that AxoNN successfully trains the model to convergence and produces near identical loss curves.

B. Weak Scaling

Let us begin with discussing the results of our weak scaling experiments on GPTs, listed in Table II. We compare the time per iteration (or batch) for AxoNN, Megatron-LM, ZeRO-3, and DeepSpeed (TP+DP+ZeRO) on Perlmutter in Figure 8 (left). On Perlmutter, we observe that AxoNN has the lowest time per iteration for all models and GPU counts. For instance, AxoNN shows improvements in the range of 25–45% over Megatron-LM. For GPT 10B, 20B, and 40B, AxoNN performs better than the second best performing method ZeRO-3, with improvements in the range of 10–18%. However, for GPT 80B on 1024 GPUs, ZeRO-3 stops scaling efficiently, and AxoNN demonstrates a 55% improvement over ZeRO-3 while scaling efficiently. Figure 8 (right) shows the performance of AxoNN, ZeRO-3, and DeepSpeed on Frontier. Similar to Perlmutter, AxoNN demonstrates the lowest time per iteration for all models and GPU counts on Frontier for GPT 40B, and 80B.

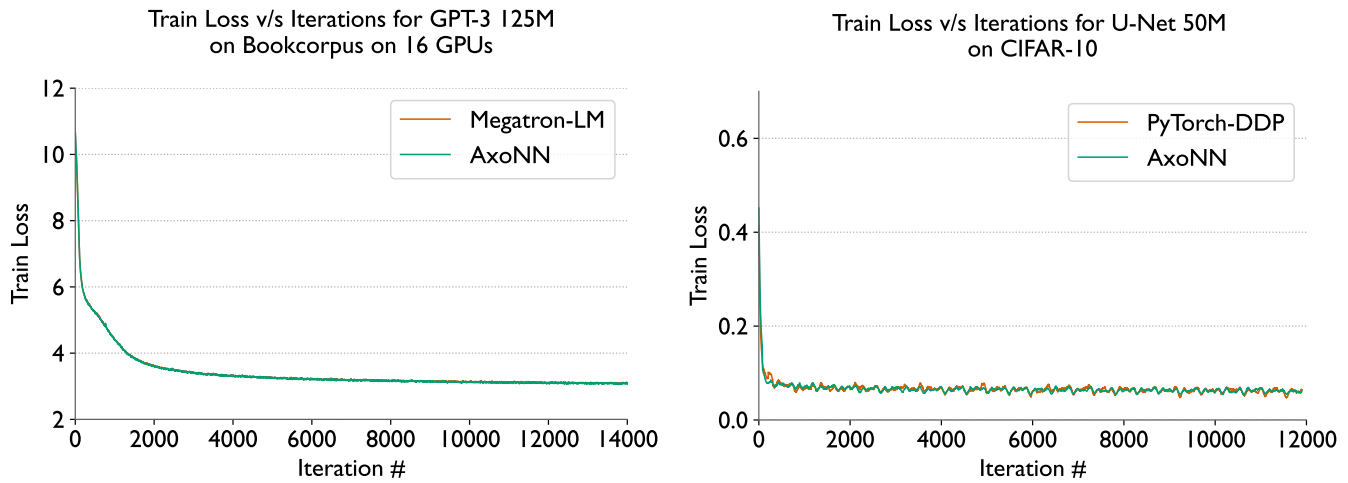


Fig. 7: Validating our implementation of AxoNN. The left figure demonstrates the training loss for AxoNN and Megatron-LM on a 125M parameter GPT-3 [3] model on 16 GPUs of Perlmutter on the BookCorpus dataset [40]. Whereas, the right figure demonstrates the training loss for AxoNN and PyTorch-DDP on a 50M parameter U-Net [28] on the CIFAR-10 dataset [37].

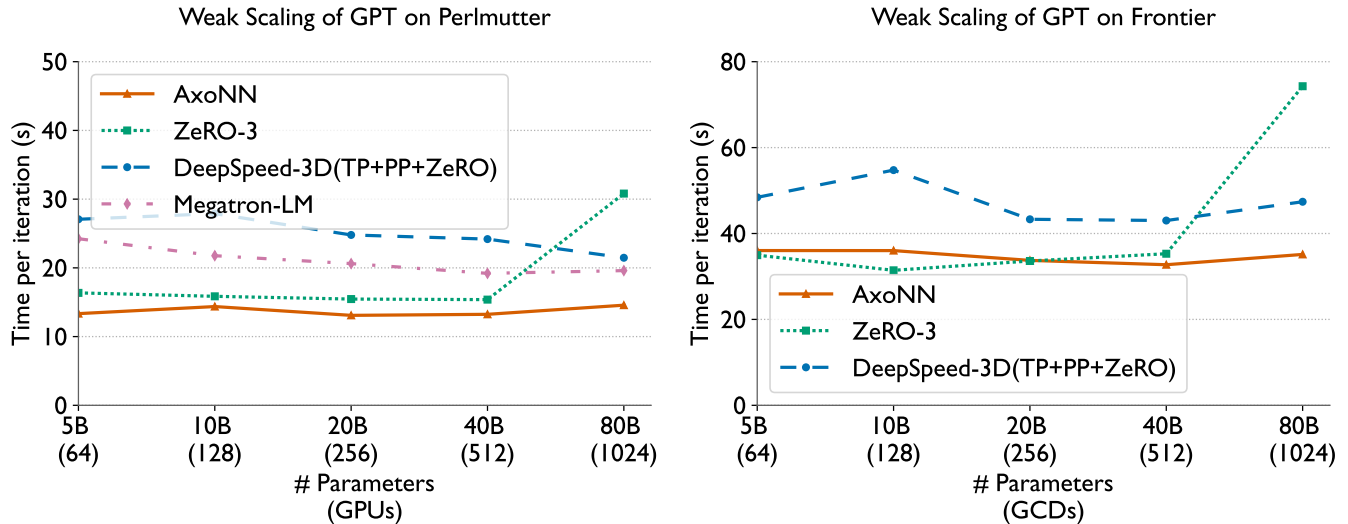


Fig. 8: Time per iteration for strong scaling of GPT transformers on Perlmutter (left) and Frontier (right). We use a batch size of 4M tokens and a sequence length of 2048.

For GPT 5B, 10B, and 20B, ZeRO-3 outperforms AxoNN by a small margin. However, with increasing GPU counts, ZeRO-3 stops scaling efficiently, while AxoNN continues to scale efficiently. In terms of scaling, AxoNN is the best performing method for all models and GPU counts on Perlmutter and Frontier, followed by Megatron-LM on Perlmutter and DeepSpeed on Frontier.

Table IV lists the hardware flop/s utilization for GPTs on Perlmutter. We notice that all method AxoNN demonstrates the highest utilization for almost all models and GPU counts, with a significantly high 57% of the peak half precision flop/s at 1024 GPUs of Perlmutter, which is nearly 16% of the machine! This is much higher than the next fastest framework - Megatron-LM, which clocks a significantly lower 42% of

the peak.

Now, we turn our attention to the Figure 10 (left) which shows the weak scaling performance of AxoNN and ZeRO-3 for U-Nets on Perlmutter (left) and Frontier (right). We observe that AxoNN is significantly faster than ZeRO-3 for all U-Net models and GPU counts. On higher GPU counts of 512 and 1024, AxoNN is upto 5 times faster than ZeRO-3 on both machines. We believe the reason for this is the flexibility of our approach to allow for different degrees of tensor parallelism. It can be shown that ZeRO-3's parallelism is equivalent to the depth tensor parallelism in our approach. For larger model sizes and higher GPU counts, depth tensor parallel dimension alone may not be sufficient to achieve good performance. This is where our approach that allows for

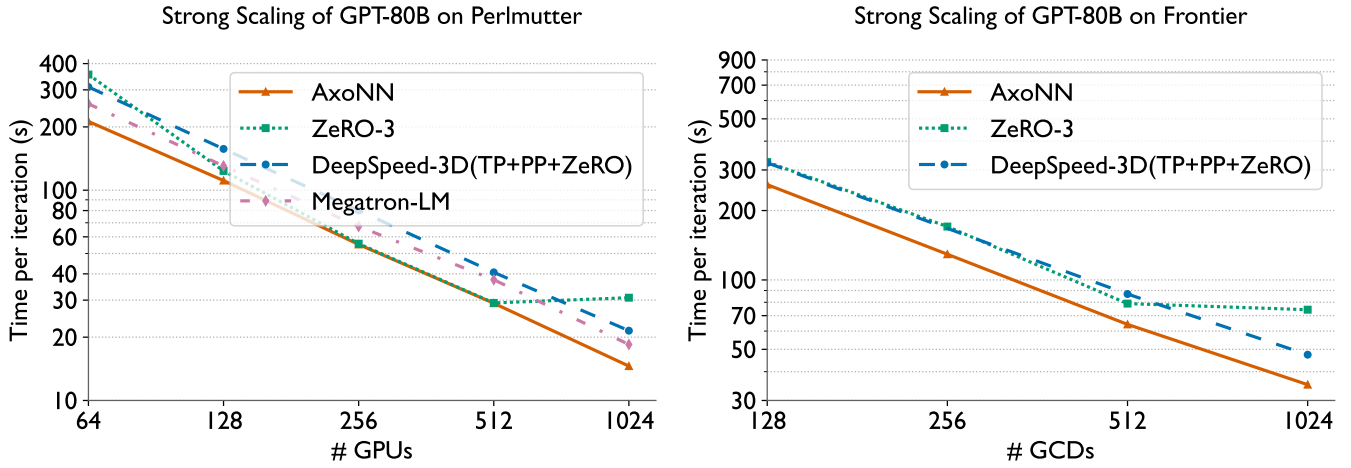


Fig. 9: Time per iteration for strong scaling of GPT-80B on Perlmutter (left) and Frontier (right). We use a batch size of 4M tokens and a sequence length of 2048.

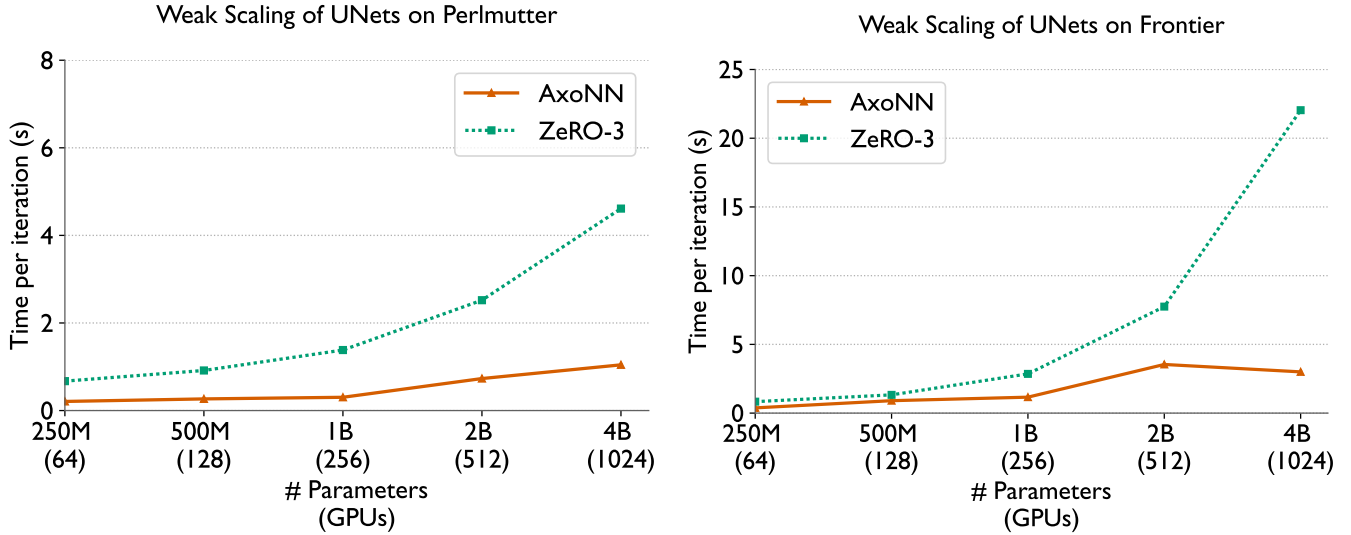


Fig. 10: Time per iteration for weak scaling of UNets on Perlmutter (left) and Frontier (right). We use a batch size of 2048 samples.

different degrees of tensor parallelism, and our communication model that finds the optimal degree of tensor parallelism, proves to be beneficial. Indeed, we see that the best performing configuration for U-Net 4B on 1024 GCDs of Frontier is $G_c = 8, G_r = 2, G_d = 16$, and $G_{data} = 8$, validating the need for different degrees of tensor parallelism.

C. Strong Scaling

Next, we demonstrate the results of our strong scaling experiments on the GPT 80B architecture in Figure 9 for Perlmutter (left) and Frontier (right). On Perlmutter, we observe that AxoNN, Megatron-LM, and DeepSpeed scale linearly upto 1024 GPUs. ZeRO-3 scales extremely well upto 512 GPUs matching AxoNN’s iteration times, but degrades significantly at 1024 GPUs. AxoNN once again demonstrates the lowest time per iteration for the GPU counts. On Frontier, AxoNN

and DeepSpeed scale almost linearly upto 1024 GCDs, while ZeRO-3 does not scale efficiently at all. AxoNN demonstrates the lowest time per iteration for all GCD counts on Frontier.

VIII. CONCLUSION

Communication overhead remains a major hurdle in distributed training of large neural networks. To overcome these limitations, we introduced AxoNN, a novel four-dimensional (4D) hybrid parallel framework. AxoNN leverages a variation of Agarwal’s efficient parallel matrix multiplication algorithm [5], but goes beyond that by employing a two-pronged approach for communication efficiency. Firstly, we proposed communication optimizations that exploit asynchronous communication. This allows for significant overlap between communication and computation, maximizing hardware utilization during training. Secondly, we introduced a communication

model that identifies a small set of communication-optimal configurations for AxoNN. This eliminates the need for exhaustive search and streamlines the process of finding the optimal settings for a user’s specific workload. By combining an efficient parallelization approach with these communication-centric strategies, AxoNN offers a significant step forward in tackling the communication bottleneck and enabling the effective training of large-scale neural networks on distributed systems.

REFERENCES

- [1] M. Belkin, D. Hsu, S. Ma, and S. Mandal, “Reconciling modern machine-learning practice and the classical bias-variance trade-off,” *Proceedings of the National Academy of Sciences*, vol. 116, no. 32, pp. 15 849–15 854, 2019. [Online]. Available: <https://www.pnas.org/doi/abs/10.1073/pnas.1903070116>
- [2] J. Kaplan, S. McCandlish, T. Henighan, T. B. Brown, B. Chess, R. Child, S. Gray, A. Radford, J. Wu, and D. Amodei, “Scaling laws for neural language models,” 2020. [Online]. Available: <https://arxiv.org/abs/2001.08361>
- [3] T. B. Brown, B. Mann, N. Ryder, M. Subbiah, J. Kaplan, P. Dhariwal, A. Neelakantan, P. Shyam, G. Sastry, A. Askell, S. Agarwal, A. Herbert-Voss, G. Krueger, T. Henighan, R. Child, A. Ramesh, D. M. Ziegler, J. Wu, C. Winter, C. Hesse, M. Chen, E. Sigler, M. Litwin, S. Gray, B. Chess, J. Clark, C. Berner, S. McCandlish, A. Radford, I. Sutskever, and D. Amodei, “Language models are few-shot learners,” *CoRR*, vol. abs/2005.14165, 2020. [Online]. Available: <https://arxiv.org/abs/2005.14165>
- [4] S. Smith, M. Patwary, B. Norick, P. LeGresley, S. Rajbhandari, J. Casper, Z. Liu, S. Prabhumoye, G. Zerveas, V. Korthikanti, E. Zhang, R. Child, R. Y. Aminabadi, J. Bernauer, X. Song, M. Shoeybi, Y. He, M. Houston, S. Tiwary, and B. Catanzaro, “Using deepspeed and megatron to train megatron-turing nlg 530b, a large-scale generative language model,” 2022. [Online]. Available: <https://arxiv.org/abs/2201.11990>
- [5] R. C. Agarwal, S. M. Balle, F. G. Gustavson, M. Joshi, and P. Palkar, “A three-dimensional approach to parallel matrix multiplication,” *IBM Journal of Research and Development*, vol. 39, no. 5, pp. 575–582, 1995.
- [6] M. Shoeybi, M. Patwary, R. Puri, P. LeGresley, J. Casper, and B. Catanzaro, “Megatron-lm: Training multi-billion parameter language models using model parallelism,” 2020.
- [7] Microsoft, “3d parallelism with megatronlm and zero redundancy optimizer,” https://github.com/microsoft/DeepSpeedExamples/tree/master/Megatron-LM-v1.1.5-3D_parallelism, 2021.
- [8] S. Rajbhandari, J. Rasley, O. Ruwase, and Y. He, “Zero: Memory optimizations toward training trillion parameter models,” in *Proceedings of the International Conference for High Performance Computing, Networking, Storage and Analysis*, ser. SC ’20. IEEE Press, 2020.
- [9] D. Hendrycks and K. Gimpel, “Gaussian error linear units (gelus),” 2020.
- [10] B. Xu, N. Wang, T. Chen, and M. Li, “Empirical evaluation of rectified activations in convolutional network,” 2015.
- [11] Y. Wu and K. He, “Group normalization,” 2018.
- [12] J. L. Ba, J. R. Kiros, and G. E. Hinton, “Layer normalization,” 2016. [Online]. Available: <https://arxiv.org/abs/1607.06450>
- [13] S. Ioffe and C. Szegedy, “Batch normalization: Accelerating deep network training by reducing internal covariate shift,” in *Proceedings of the 32nd International Conference on Machine Learning*, ser. Proceedings of Machine Learning Research, F. Bach and D. Blei, Eds., vol. 37. Lille, France: PMLR, 07–09 Jul 2015, pp. 448–456. [Online]. Available: <http://proceedings.mlr.press/v37/ioffe15.html>
- [14] BigScience, “Bigscience large open-science open-access multilingual language model,” <https://huggingface.co/bigscience/bloom>, 2022.
- [15] D. Narayanan, M. Shoeybi, J. Casper, P. LeGresley, M. Patwary, V. Korthikanti, D. Vainbrand, P. Kashinkunti, J. Bernauer, B. Catanzaro, A. Phanishayee, and M. Zaharia, “Efficient large-scale language model training on GPU clusters,” *CoRR*, vol. abs/2104.04473, 2021. [Online]. Available: <https://arxiv.org/abs/2104.04473>
- [16] Q. Xu, S. Li, C. Gong, and Y. You, “An efficient 2d method for training super-large deep learning models,” 2021. [Online]. Available: <https://arxiv.org/abs/2104.05343>
- [17] B. Wang, Q. Xu, Z. Bian, and Y. You, “Tesseract: Parallelize the tensor parallelism efficiently,” in *Proceedings of the 51st International Conference on Parallel Processing*. ACM, aug 2022. [Online]. Available: <https://doi.org/10.1145%2F3545008.3545087>
- [18] A. Jangda, J. Huang, G. Liu, A. H. N. Sabet, S. Maleki, Y. Miao, M. Musuvathi, T. Mytkowicz, and O. Sarikivi, “Breaking the computation and communication abstraction barrier in distributed machine learning workloads,” 2022.
- [19] N. Dryden, N. Maruyama, T. Moon, T. Benson, M. Snir, and B. Van Essen, “Channel and filter parallelism for large-scale cnn training,” in *Proceedings of the International Conference for High Performance Computing, Networking, Storage and Analysis*, ser. SC ’19. New York, NY, USA: Association for Computing Machinery, 2019. [Online]. Available: <https://doi.org/10.1145/3295500.3356207>
- [20] S. Wang, J. Wei, A. Sabne, A. Davis, B. Ilbeyi, B. Hechtman, D. Chen, K. S. Murthy, M. Maggioni, Q. Zhang, S. Kumar, T. Guo, Y. Xu, and Z. Zhou, “Overlap communication with dependent computation via decomposition in large deep learning models,” in *Proceedings of the 28th ACM International Conference on Architectural Support for Programming Languages and Operating Systems, Volume 1*, ser. ASPLOS 2023. New York, NY, USA: Association for Computing Machinery, 2022, p. 93–106. [Online]. Available: <https://doi.org/10.1145/3567955.3567959>
- [21] Z. Lai, S. Li, X. Tang, K. Ge, W. Liu, Y. Duan, L. Qiao, and D. Li, “Merak: An efficient distributed dnn training framework with automated 3d parallelism for giant foundation models,” *IEEE Transactions on Parallel and Distributed Systems*, vol. 34, no. 5, pp. 1466–1478, 2023.
- [22] S. Li, Z. Lai, Y. Hao, W. Liu, K. Ge, X. Deng, D. Li, and K. Lu, “Automated tensor model parallelism with overlapped communication for efficient foundation model training,” *arXiv preprint arXiv:2305.16121*, 2023.
- [23] L. Zheng, Z. Li, H. Zhang, Y. Zhuang, Z. Chen, Y. Huang, Y. Wang, Y. Xu, D. Zhuo, J. E. Gonzalez, and I. Stoica, “Alpa: Automating inter- and intra-operator parallelism for distributed deep learning,” *CoRR*, vol. abs/2201.12023, 2022. [Online]. Available: <https://arxiv.org/abs/2201.12023>
- [24] S. Cheng, Z. Liu, J. Du, and Y. You, “Atp: Adaptive tensor parallelism for foundation models,” *arXiv preprint arXiv:2301.08658*, 2023.
- [25] A. Tripathy, K. Yelick, and A. Buluç, “Reducing communication in graph neural network training,” in *SC20: International Conference for High Performance Computing, Networking, Storage and Analysis*. IEEE, 2020, pp. 1–14.
- [26] A. Bhatele, R. Dhakal, A. Movsesyan, A. Ranjan, J. Marry, and O. Cankur, “Pipit: Enabling programmatic analysis of parallel execution traces,” 2023.
- [27] R. Rabenseifner, “Optimization of collective reduction operations,” in *Computational Science - ICCS 2004*, M. Bubak, G. D. van Albada, P. M. A. Sloot, and J. Dongarra, Eds. Berlin, Heidelberg: Springer Berlin Heidelberg, 2004, pp. 1–9.
- [28] O. Ronneberger, P. Fischer, and T. Brox, “U-net: Convolutional networks for biomedical image segmentation,” 2015. [Online]. Available: <https://arxiv.org/abs/1505.04597>
- [29] A. Ramesh, P. Dhariwal, A. Nichol, C. Chu, and M. Chen, “Hierarchical text-conditional image generation with clip latents,” 2022. [Online]. Available: <https://arxiv.org/abs/2204.06125>
- [30] R. Rombach, A. Blattmann, D. Lorenz, P. Esser, and B. Ommer, “High-resolution image synthesis with latent diffusion models,” 2021. [Online]. Available: <https://arxiv.org/abs/2112.10752>
- [31] S. Minaee, Y. Boykov, F. Porikli, A. Plaza, N. Kehtarnavaz, and D. Terzopoulos, “Image segmentation using deep learning: A survey,” *IEEE Transactions on Pattern Analysis and Machine Intelligence*, vol. 44, no. 7, pp. 3523–3542, 2022.
- [32] L. Jiao, F. Zhang, F. Liu, S. Yang, L. Li, Z. Feng, and R. Qu, “A survey of deep learning-based object detection,” *IEEE Access*, vol. 7, pp. 128 837–128 868, 2019. [Online]. Available: <https://doi.org/10.1109%2FAccess.2019.2939201>
- [33] A. Vaswani, N. Shazeer, N. Parmar, J. Uszkoreit, L. Jones, A. N. Gomez, L. Kaiser, and I. Polosukhin, “Attention is all you need,” *CoRR*, vol. abs/1706.03762, 2017. [Online]. Available: <http://arxiv.org/abs/1706.03762>
- [34] A. Radford, J. Wu, R. Child, D. Luan, D. Amodei, and I. Sutskever, “Language models are unsupervised multitask learners,” 2019.
- [35] T. Chen, B. Xu, C. Zhang, and C. Guestrin, “Training deep nets with sublinear memory cost,” 2016.

- [36] A. Nichol and P. Dhariwal, "Improved denoising diffusion probabilistic models," 2021.
- [37] A. Krizhevsky, V. Nair, and G. Hinton, "Cifar-10 (canadian institute for advanced research)." [Online]. Available: <http://www.cs.toronto.edu/~kriz/cifar.html>
- [38] L. AI, "Litgpt," <https://github.com/Lightning-AI/litgpt>, 2023.
- [39] Microsoft, "Deepspeed: Extreme-scale model training for everyone," <https://www.microsoft.com/en-us/research/blog/deepspeed-extreme-scale-model-training-for-everyone/>.
- [40] Y. Zhu, R. Kiros, R. Zemel, R. Salakhutdinov, R. Urtasun, A. Torralba, and S. Fidler, "Aligning books and movies: Towards story-like visual explanations by watching movies and reading books," in *arXiv preprint arXiv:1506.06724*, 2015.